Received: 20 October 2023 | Revised: 6 November 2023 | Accepted: 6 November 2023

DOI: 10.1111/jace.19646

Journal of the American Ceramic Society

RAPID COMMUNICATION

Calcium–magnesium–aluminum-silicate melt viscosities influenced by lanthanides, yttrium, and zirconium

Dirk Müller | **Donald B. Dingwell**

Department for Earth and Environmental Sciences, LMU Munich, Munich, Germany

Correspondence
Dirk Müller, Department for Earth and Environmental Sciences, LMU Munich, Theresienstrasse 41, 80333 Munich, Germany.
Email: dirk.mueller@lmu.de

Funding information
ERC, Grant/Award Number: 2018 ADG 834225

Abstract

Lanthanides (Ln_2O_3) and elements like Zr and Y find application in the highest temperature-resistant thermal and/or environmental barrier coatings. Such coatings are routinely exposed to silicate particles (e.g., sand, dust, volcanic ash), leading to chemical reactions that degrade the coating. The dissolution of 13.5 wt.% Ln_2O_3 into a calcium–magnesium–aluminum-silicate (CMAS) melt leads to a viscosity reduction for the light lanthanides, while viscosity increases toward heavier lanthanides. For Gd, Y, and Zr, various amounts up to 13.5 wt.% (Gd_2O_3, Y_2O_3, ZrO_2) were added to the CMAS melt, showing a tendency of increased viscosity for low concentrations (2.5-3 wt.%) and a decreasing viscosity for higher values of the added component.

KEYWORDS
cerium, environmental barrier coating, europium, rare earth elements, thermal barrier coating

1 | INTRODUCTION

In the push toward ever higher turbine temperatures in order to increase combustion efficiency, the state-of-the-art TBC material of yttria-stabilized zirconia (YSZ; 7–8 wt.% Y_2O_3 doped ZrO_2) has reached its limits of stability[1] and is going to be replaced by alternative materials. New technologies involving phases with major element concentrations of lanthanides (i.e., jet turbine thermal barrier coatings/environmental barrier coatings [T/EBCs]) have thrust the need for a proper and systematic set of parametrizations of the properties of lanthanides in silicate phases into the global research spotlight.[2–4] Many of these applications appeal to the extremely high-temperature stability and low thermal conductivity of lanthanide-based ceramics.[5] However, a major drawback is their potential susceptibility to chemical "attack" (i.e., chemical reaction between lanthanide-based ceramics and silicate melts).[5–13] The interaction between a silicate melt and TBC/EBC is characterized by a (partial) dissolution of the coating and/or the leaching of specific elements from the coating into the melt.[14,15] Viscosity is the dominating melt property influencing the successive stages (e.g., spreading and infiltration) of the physical interaction of silicate melts and TBCs / EBCs,[15–17] while It also serves as an inverse proxy for the diffusivities of several major chemical components of these reacting systems.[18] In recent studies the impact of YSZ and gadolinium zirconate (GZO) dissolved into (1) volcanic ash melts [19] and (2) calcium-magnesium-aluminum-silicate (CMAS) melts [20] on the viscosities of the melts at high temperatures have been investigated. For all the volcanic ash melts the dissolution of YSZ and GZO leads to a significant reduction of viscosity, whereas for the CMAS melts the viscosity change depends on the chemical composition of the melt, the temperature, and the dopant (YSZ, GZO) amount. In order to rationalize and be able

to generalize these results, we have recognized the need for a systematic set of synthetic studies of the influence of the individual major components of TBC/EBCs on the viscosity of silicate melt compositions.

2 | MATERIALS AND METHODS

2.1 | Synthesis of the materials

The base material for this study is a CMAS consisting of CaO (33.16 wt.%), MgO (6.50 wt.%), Al_2O_3 (11.88 wt.%), and SiO_2 (48.46 wt.%). This CMAS composition represents the composition published by Borom et al.,[21] and was already used for a previous study,[20] where YSZ or GZO were added in order to investigate the viscosity change of the melt.

Two series of CMAS samples were prepared (Supporting Material S1):

(a) CMAS + 13.5 wt.% Ln_2O_3 (excluding Pm)
(b) CMAS + two series of 3, 6.5, 10, 13.5 wt.% Gd_2O_3 and Y_2O_3 and one series of 2.5, 6.5, 8.5, 13.5 wt.% ZrO_2.

The feedstock powders for synthesis were a calcium carbonate ($CaCO_3$—Merck, ≥98.5%) for Ca and pure oxides for Mg, Al, Si, Y, Zr and the lanthanides (MgO—Merck, p.a., ≥97 %; Al_2O_3—Merck, ≥99 %; SiO_2 – ChemPUR, 99.9%; Y_2O_3—ChemPUR, 99.9%; ZrO_2—ChemPUR 99.995% with 0.5% Hf; La_2O_3—Alfa Aesar, 99.9%; CeO_2—ChemPUR, 99.99%; Pr_6O_{11}—Alfa Aesar, 99.9%; Nd_2O_3—Alfa Aesar, 99.9%; Sm_2O_3—Alfa Aesar, 99.99%; Eu_2O_3—ChemPUR, 99.9%; Gd_2O_3—Alfa Aesar, 99.9%; Tb_4O_7—Alfa Aesar, 99.9%; Dy_2O_3—Alfa Aesar, 99.9%; Ho_2O_3—ChemPUR, 99.99%; Er_2O_3—Alfa Aesar, 99.9%; Tm_2O_3—ChemPUR, 99.99%; Yb_2O_3—Alfa Aesar, 99.9%; Lu_2O_3—ChemPUR 99.9%). These powders were dried at 110°C overnight before they were weighed to get the appropriate compositions. The lanthanides were assumed to be present in a 3+ oxidation state at high temperatures,[22] so that the required amounts of CeO_2, Pr_6O_{11}, and Tb_4O_7 were recalculated.

The resulting powder mixtures were transferred into thin-walled Pt-crucibles and put into a Nabertherm furnace at 1400°C for 1 h. To obtain glasses for viscometry the melt was removed from the furnace and quenched on a stainless-steel plate.

2.2 | Viscometry

Each of the previously synthesized glasses was remelted in a $Pt_{80}Rh_{20}$ thick-walled viscometry crucible and then transferred into a viscometry furnace. Viscosity determination was carried out by continuously recording the torque of a $Pt_{80}Rh_{20}$ spindle immersed in the melt while temperature was stepwise reduced by 25°C starting from the highest temperature of 1490°C (1587°C for sample S4 Zr 13.5). [23,24] Measurement stopped when crystallization of the melt occurred or the limits of the instrument were reached. To check for instrument drift each sample was reheated to the initial temperature of 1490°C (1587°C) and the viscosity was redetermined. Postexperiment the samples were subsequently removed from the furnace and quenched in air. For calibration, the standard DGG-1[25] was used.

2.3 | Electronprobe microanalysis

Chips of the post-viscometry glasses were prepared for electronprobe microanalysis (EPMA) and measured with a Cameca SX-100 microprobe. Analytical conditions were 15 kV, 5 nA, and a defocused beam of 10 μm. The following standards were used: wollastonite (Ca), periclase (Mg), synth. Al_2O_3 (Al), albite (Si), cubic zirconia (Y, Zr), and rare earth phosphates for the lanthanides.

3 | RESULTS

The postviscometry glass chips were analyzed by EPMA, confirming the stoichiometry of the weight compositions within a relative error of 3 % (Supporting Material S1).

3.1 | Constant Ln_2O_3 dopant level of 13.5 wt.%

For the purpose of easier identification, the lanthanides are separated into two groups of seven elements roughly representing the light rare earths (LREE; La, Ce, Pr, Nd, Sm, Eu, Gd) and the heavy rare earths (HREE; Tb, Dy, Ho, Er, Tm, Yb, Lu; Figure 1). Figure 1A1 and A2 show the viscosities of all 13.5 wt.% lanthanide doped CMAS melts as well as the undoped CMAS melt in relation to the temperature in an Arrhenian plot (logarithmic viscosity versus reciprocal absolute temperature). In Figure 1B1 and B2, the differences in viscosity ($\Delta\log\eta = \log\eta_{Ln2O3\ doped} - \log\eta_{pure}$) versus the temperature are shown. The effect of the lanthanide doping can mostly be considered to be viscosity decreasing. However, the slight nonlinearity indicates a non-Arrhenian behavior for all samples (doped and undoped). This curvature, also describable as the fragility of the sample, is stronger for the lanthanide-doped samples leading to a viscosity crossover at lower temperatures with the undoped CMAS melt. This crossover is responsible for a viscosity-increasing effect of the HREE toward lower temperatures (Figure 1B2). Notably, viscometry of the

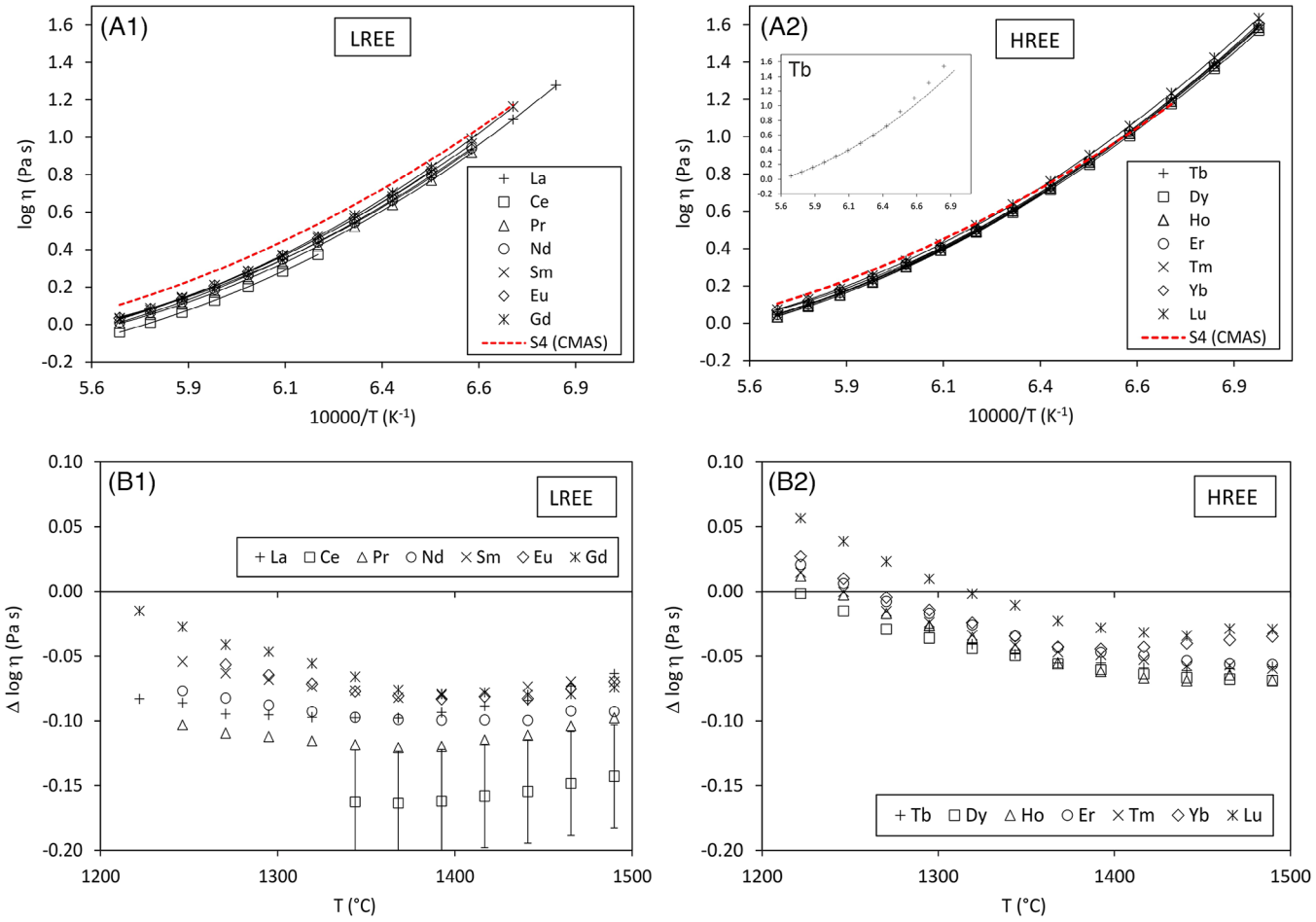

FIGURE 1 (A1 and A2) Arrhenian viscosity plots for the pure CMAS melt (dashed line) and the lanthanide-doped CMAS melts. The error of ±0.02 Pa s is roughly represented by the symbol size. (B1 and B2) Delta viscosity plots (Δlog η vs. temperature) for all lanthanide-doped CMAS melts. The error of ±0.04 Pa s is only shown for the Ce sample, while it is valid for all data points. For simplicity the lanthanide dopants are only labeled as elements, while they are considered as oxides (Ln_2O_3).

Tb-doped CMAS melt was difficult, so that reliable data could only be obtained between a temperature of 1490–1319°C. At lower temperatures, the viscosity of the Tb-doped sample drifts away from the high-temperature trend (inset in Figure 1A2). On a first inspection of Figure 2, it appears that viscosity linearly correlates with the atomic number, with the exception of Ce. However, this observation needs to be seen in the light of a constant lanthanide doping level of 13.5 wt.%, leading to shifting molar concentrations from 2.78 mol% (La_2O_3) to 2.29 mol% (Lu_2O_3).

3.2 | Varying dopant levels of Gd_2O_3, Y_2O_3, and ZrO_2

In Figure 3A1, A2, and A3 the Arrhenian plots of the Gd_2O_3, Y_2O_3, and ZrO_2 doped CMAS melts are shown. Comparable with the lanthanide doped samples (Figure 1) all curves show a non-Arrhenian behavior, leading to a crossover effect for most of the doped samples with the undoped CMAS sample. Exceptions from that crossover are sample Y 3 (3 wt.% Y_2O_3) and Zr 2.5 (2.5 wt.% ZrO_2). For the Gd_2O_3 doped samples, the differences between the 3, 6.5, and 10 wt.% doping amounts are negligible, with respect to the error of ±0.02 log Pa s, whereas Gd 13.5 shows a significantly reduced viscosity (Figure 3A1). In contrast, the viscosity of the Y_2O_3 doped samples continuously decreases in a significant manner with increasing dopant amount (Figure 3A2). ZrO_2-doped samples only gave reasonable viscosity data for a dopant amount of up to 8.5 wt.% ZrO_2 (Figure 3A3). Viscosities for sample Zr 13.5 were only obtainable at temperatures above 1539°C (Supporting Material S2). Sample Zr 8.5 has the lowest viscosity at temperatures above ~1400°C, whereas the Δlog η shows a strong curvature toward lower temperatures, leading to a crossover with sample Zr 6.5 (Figure 3B3). The sample doped with 2.5 wt.% ZrO_2 shows an overall increased viscosity.

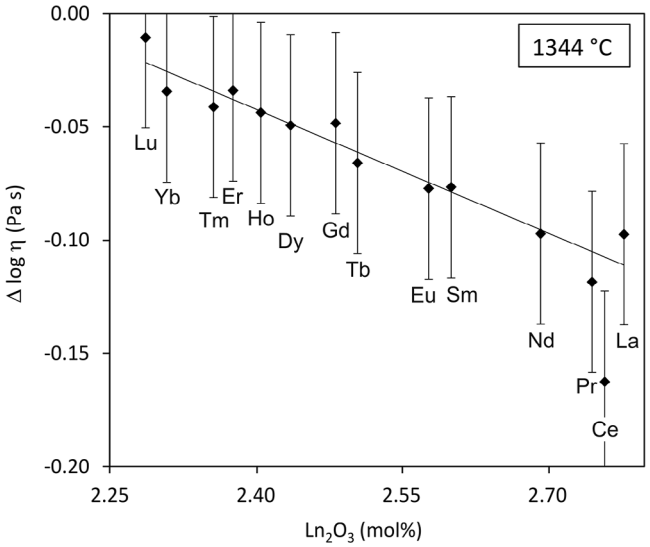

FIGURE 2 Delta viscosity plot (Δlog η vs. Ln_2O_3 amount) at a temperature of 1344°C. For simplicity the dopants are only labeled as elements, while they are considered as oxides (Ln_2O_3).

As two general trends for CMAS doped with varying amounts of Gd_2O_3, Y_2O_3, and ZrO_2 it can be observed that (1) the viscosity differences between various dopant amounts become more pronounced toward higher temperatures and (2) the viscosity increases from Gd to Y to Zr doping of the CMAS melt.

4 | DISCUSSION

The influence of lanthanide addition to CMAS melt viscosity results in an overall decreased viscosity for the addition of LREE (La–Gd), whereas the addition of HREE (Tb–Lu) leads to a decreased viscosity at high temperatures only and an increased viscosity toward lower temperatures. These observations correlate with the influence of YSZ or GZO additions to a CMAS melt with the same composition (sample S4 in Müller and Dingwell[20]) as well as with the addition of Ln_2O_3 to a sodium disilicate (NS_2) melt.[26]

Chemical reactions between T/EBC materials and silicate melts at high temperatures can lead to phase changes (e.g., tetragonal YSZ → cubic/monoclinic YSZ), formation of new crystalline phases (e.g., REE-apatite/REE-fluorite/REE-garnet phases) and/or a full disintegration of the coating.[4,15,27] Such reactions lead to an enrichment of the coating elements (e.g., lanthanides, Zr, Y) within the silicate melt, modifying its physicochemical properties, like viscosity. Since viscosity is the dominating factor for the wetting and spreading ability of the melt,[15–17] it is crucial to understand the impact of coating elements on the melt viscosity in order to estimate the potentially affected T/EBC regions. However, for a transfer of these laboratory data to the application environment (T/EBCs in turbines), it needs to be considered that especially the chemical composition of the initial melt as well as the amount of dissolved lanthanides and the temperature strongly influence the viscosity changes: (1) natural volcanic ash behaves differently in comparison to synthetic volcanic ash and CMAS representatives [19,20]; (2) due to the amphoteric character of the lanthanides their influence on viscosity depends on their amount (Figure 3 and Müller and Dingwell[20]); (3) as the fragility (curvature within the Arrhenian plot) is different for pure and doped silicate melts, the resulting crossover (Figures 1 and 3) leads to viscosity increasing or decreasing regimes for specific dopants (Figures 1 and 3 and compare Müller et al.[26]).

Based on previous studies from Cicconi[28] and Cicconi et al.,[29] it can be assumed that Ce and Eu are present in multivalent states ($Ce^{3+/4+}$; $Eu^{2+/3+}$), what possibly impacts the melt viscosities of the respective samples, whereas other lanthanides are expected to be present in 3+ valence state.[22] For the Ce-modified sample a significant difference is observable, as its viscosity is too low in comparison to the neighboring samples, whereas for the Eu-modified sample, no irregularity can be identified. For a discussion of these two phenomena, the $Eu^{2+}/(Eu^{2+} + Eu^{3+})$ and $Ce^{4+}/(Ce^{3+} + Ce^{4+})$ ratios were calculated based on equations from Burnham et al.[30] and Pinet et al.,[31] respectively:

$$\frac{Eu^{2+}}{Eu^{2+}+Eu^{3+}} = 1 - \frac{1}{1+10^{\left(-0.25\ \log fO_2 - \frac{6410}{T} - 14.2\ \Lambda + 10.1\right)}}, \quad (1)$$

$$\frac{Ce^{4+}}{Ce^{3+}+Ce^{4+}} = 1 - \frac{10^{\left(4.319 - \frac{3328}{T} - 3.631*\Lambda - 0.25\log fO_2\right)}}{1+10^{\left(4.319 - \frac{3328}{T} - 3.631*\Lambda - 0.25\log fO_2\right)}}, \quad (2)$$

where m_{Ln2O3} denotes the Ln_2O_3 dopant amount (13.5 wt.%), T for the temperature in K, fO_2 for the oxygen fugacity (0.21 in air), and Λ for the optical basicity. For the calculation of the optical basicities of the lanthanide-doped melts, the following optical basicities of the oxides were taken: CaO, 1.00; MgO, 0.78; Al_2O_3,0.60; SiO_2, 0.48; Eu_2O_3, 1.099; Ce_2O_3, 1.176, taken from Duffy[32] and Duffy.[33] The "normal" behavior of the Eu modified sample can most probably be explained by the small concentration Eu^{2+} in the CMAS melt ($Eu^{2+}/(Eu^{2+}+Eu^{3+})$ = 0.13% at 1344°C; Figure 4), so that its potentially viscosity modifying impact is overprinted by the error of viscosity measurement (± 0.02 log Pa s). Higher concentrations of Eu^{2+} might be achievable for melt compositions with lower optical basicities since decreasing basicity would lead to an increasing reduction potential of the melt.[34] Following the cationic field strength (CFS) theory, an increasing presence of Eu^{2+} should result in decreasing viscosity, since lower CFS values (CFS_{Eu2+} = 0.31 $Å^{-2}$; CFS_{Eu3+} = 0.55 $Å^{-2}$) should lead to lower viscosities.[35] The observable viscosity reduction through the addition

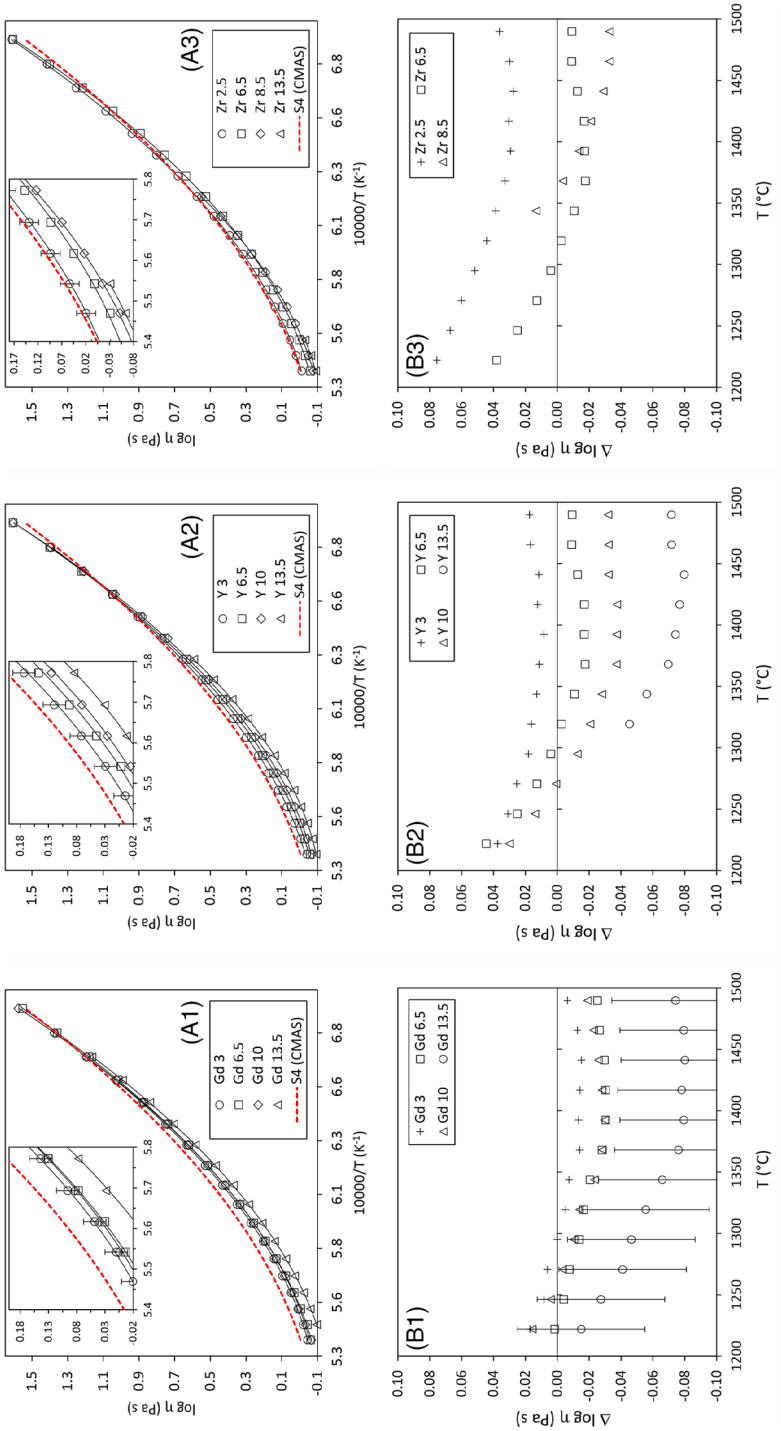

FIGURE 3 (A1, A2, and A3) Arrhenian viscosity plots for the pure S4 CMAS melt (dashed line) and the Gd_2O_3-, Y_2O_3-, and ZrO_2-doped S4 CMAS melts. The error of ±0.02 Pa s is roughly represented by the symbol size. The insets represent an enlarged view of the high-temperature regions. (B1, B2, and B3) Delta viscosity plots ($\Delta \log \eta$ vs. temperature) for the Gd_2O_3-, Y_2O_3-, and ZrO_2-doped S4 CMAS melts. (C1, C2, and C3) Delta viscosity plots ($\Delta \log \eta$ vs. Gd-, Y-, Zr-oxide amount) for the Gd_2O_3-, Y_2O_3-, and ZrO_2-doped S4 CMAS melts. For simplicity, the dopants are only labeled by their cation, while they are considered as oxides (Gd_2O_3, Y_2O_3, ZrO_2). The error bars (±0.04 Pa s) of the delta viscosity plots (B1-3, C1-3) are only shown for one sample, while they are valid for all data points.

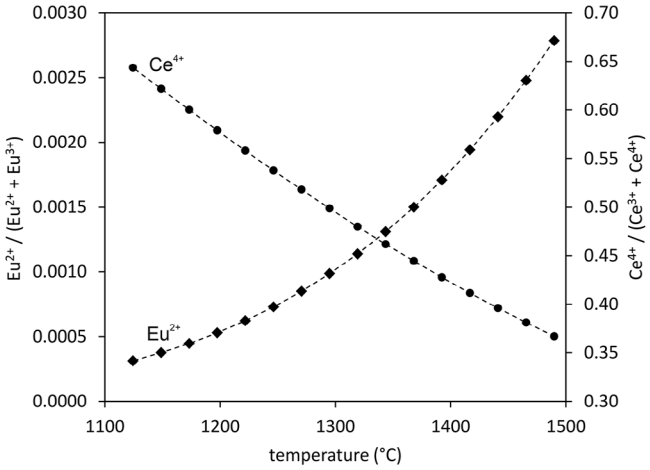

FIGURE 4 Comparison between relative Eu^{2+} and Ce^{4+} concentrations in the CMAS melt in a temperature range of 1125–1490°C.

of Ce_2O_3, however, contradicts the CFS theory, since the assumed presence of significant amounts of Ce^{4+} in the CMAS melt (Figure 4) should lead to higher viscosities (CFS_{Ce4+} = 0.79 $Å^{-2}$; CFS_{Ce3+} = 0.53 $Å^{-2}$). This observation for Ce-modified silicate melts corresponds with studies from Guo et al.[36] and Müller et al.,[26] suggesting that the pure presence of multiple valence states can lead to lower viscosities.

CMAS samples, doped with varying amounts of Gd_2O_3, Y_2O_3, and ZrO_2 compare very well with previous studies of YSZ and GZO modified CMAS melts with the same CMAS composition.[20] The curved lines in Figure 3 C1–3 are an expression of the amphoteric character of Gd, Y, and Zr[35,37] with an acidic behavior at lower concentrations and more basic behavior at higher concentrations,[37–39] that leads to the changing impact on CMAS melt viscosities from an increased toward a decreased regime (from low to high concentrations). Notably, Gd, Y, and Zr nicely follow the CFS theory, as the viscosity of the modified samples increases from Gd (CFS = 0.568 $Å^{-2}$) to Y (CFS = 0.587 $Å^{-2}$) to Zr (CFS = 0.812 $Å^{-2}$). However, for the ZrO_2-doped samples only a limited statement can be given due to crystallization phenomena at higher dopant amounts. Even though the 8.5 wt.% ZrO_2 doped sample shows no obvious deviations of the viscometry signal in a temperature range between 1490°C and 1344°C, it reveals a different behavior in comparison to the samples with lower dopant amounts of 3 and 6.5 wt.% ZrO_2 (Figure 3).

5 | CONCLUSION

In any high-temperature interaction between silicate melts and TBCs/EBCs containing significant fractions of refractory elements (lanthanides, Y, Zr), the immediate effect of dissolution of the TBC/EBC into the melt phase will be a changing melt viscosity, thereby influencing further physicochemical interaction. Enhanced spreading and infiltration will be most severe at higher system temperatures and higher concentrations of the dissolved element.

Those results differ from the viscosities of YSZ/GZO-doped natural volcanic ejecta[19] that show that complex natural chemical compositions behave differently, emphasizing the need for extensive data of lanthanide-modified natural 10-component remelted volcanic ash samples.

ACKNOWLEDGEMENTS

The authors thank Norbert Grahle-Jacobs for EPMA sample preparation. DBD acknowledges support of the ERC 2018 ADG 834225 (EAVESDROP).

Open access funding enabled and organized by Projekt DEAL.

ORCID

Dirk Müller https://orcid.org/0000-0002-9681-1056

REFERENCES

1. Krogstad JA, Krämer S, Lipkin DM, Johnson CA, Mitchell DRG, Cairney JM, et al. Phase stability of t'-zirconia-based thermal barrier coatings: mechanistic insights. J Am Ceram Soc. 2011;94:168–77. https://doi.org/10.1111/j.1551-2916.2011.04531.x
2. Tian Z, Zhang J, Zhang T, Ren X, Hu W, Zheng L, et al. Towards thermal barrier coating application for rare earth silicates RE_2SiO_5 (RE = La, Nd, Sm, Eu, and Gd). J Eur Ceram Soc. 2019;39:1463–76. https://doi.org/10.1016/j.jeurceramsoc.2018.12.015
3. Tejero-Martin D, Bennett C, Hussain T. A review on environmental barrier coatings: history, current state of the art and future developments. J Eur Ceram Soc. 2020;41:1747–68. https://doi.org/10.1016/j.jeurceramsoc.2020.10.057
4. Praveen K, Shanmugavelayutham G, Srinivasa Rao D, Sivakumar G. Development of lanthanum cerate based thermal barrier coatings with enhanced resistance to ingestion by volcanic ash particles. Corros Sci. 2022;195:109948. https://doi.org/10.1016/j.corsci.2021.109948
5. Pan W, Phillpot SR,Wan C,Chernatynskiy A,Qu Z. Low thermal conductivity oxides. MRS Bull. 2012;37:917–22. https://doi.org/10.1557/mrs.2012.234
6. Lee KN, Fox DS, Bansal NP. Rare earth silicate environmental barrier coatings for SiC/SiC composites and Si3N4 ceramics. J Eur Ceram Soc. 2005;25:1705–15. https://doi.org/10.1016/j.jeurceramsoc.2004.12.013
7. Bakan E, Vaßen R. Ceramic top coats of plasma-sprayed thermal barrier coatings: materials, processes, and properties. J Therm Spray Technol. 2017;26:992–1010. https://doi.org/10.1007/s11666-017-0597-7
8. Tian Z, Zhang J, Zheng L, Hu W, Ren X, Lei Y, et al. General trend on the phase stability and corrosion resistance of rare earth monosilicates to molten calcium-magnesium-aluminosilicate at

1300°C. Corros Sci. 2019;148:281–92. https://doi.org/10.1016/j.corsci.2018.12.032

9. Boissonnet G, Chalk C, Nicholls J R, Bonnet G, Pedraza F. Phase stability and thermal insulation of YSZ and erbia-yttria co-doped zirconia EB-PVD thermal barrier coating systems. Surf Coat Technol. 2020;389:125566. https://doi.org/10.1016/j.surfcoat.2020.125566
10. Ren K, Wang Q, Shao G, Zhao X, Wang Y. Multicomponent high-entropy zirconates with comprehensive properties for advanced thermal barrier coatings. Scr Mater. 2020;178:382–86. https://doi.org/10.1016/j.scriptamat.2019.12.006
11. Turcer LR, Padture NP. Rare-earth pyrosilicate solid-solution environmental-barrier coating ceramics for resistance against attack by molten calcia-magnesia-aluminosilicate (CMAS) glass. J Mat Res. 2020;35:2373–84. https://doi.org/10.1557/jmr.2020.132
12. Bedoya-Trujillo IF, Pérez S, Guijosa-García CY, Rivera-Gil MA, Naraparaju R, Zárate-Medina J, et al. Evaluation of the reactivity of dense lanthanum-gadolinium zirconate ceramics with Colima volcanic ashes. Surf Coat Technol. 2023;470:129825. https://doi.org/10.1016/j.surfcoat.2023.129825
13. Godbole E P, Hewage N, von der Handt A, Poerschke D L. Quantifying the efficieny of reactions between silicate melts and rare earth aluminate-zirconaze T/EBC materials. J Eur Cer Soc. 2023;43:5626–35. https://doi.org/10.1016/j.jeurceramsoc.2023.05.009
14. Rivera-Gil MA, Gomez-Chavez JJ, Ramana CV, Naraparaju R, Schulz U, Munoz-Saldana J. High temperature interaction of volcanic ashes with 7YSZ TBC's produced by APS: infiltration behavior and phase stability, Surf Coat Technol. 2019;378:124915. https://doi.org/10.1016/j.surfcoat.2019.124915
15. Müller D, Hess K-U, Kueppers U, Lokachari S, Dingwell DB, Wolf G, et al. Rheological and chemical interaction between volcanic ash and thermal barrier coatings. Surf Coat Technol. 2021;412:127049. https://doi.org/10.1016/j.surfcoat.2021.127049
16. Song W, Lavallée Y, Wadsworth F B, Hess K-U, Dingwell DB. Wetting and spreading of molten volcanic ash in jet engines. J Phys Chem Lett. 2017;8:1878–84. https://doi.org/10.1021/acs.jpclett.7b00417
17. Yang S, Song W, Lavallée Y, Zhou X, Dingwell DB, Guo H. Dynamic spreading of re-melted volcanic ash bead on thermal barrier coatings. Corros Sci. 2020;170:108659. https://doi.org/10.1016/j.corsci.2020.108659
18. Dingwell DB. Effects of structural relaxation on cationic tracer diffusion in silicate melts. Chem Geol. 1990;82:209–16. https://doi.org/10.1016/0009-2541(90)90082-I
19. Müller D, Hess K-U, Kueppers U, Dingwell DB. Effects oft he dissolution of thermal barrier coating materials on the viscosity of remelted volcanic ash. Am Min. 2020;105:1104–7. https://doi.org/10.2138/am-2020-7334
20. Müller D, Dingwell DB. The influence of thermal barrier coating dissolution on CMAS melt viscosities. J Eur Ceram Soc. 2021;41:2746–52. https://doi.org/10.1016/j.jeurceramsoc.2020.11.037
21. Borom MP, Johnson CA, Peluso LA. Role of environmental deposits and operating surface temperature in spallation of air plasma sprayed thermal barrier coatings. Surf Coat Technol. 1996;86-87:116–26. https://doi.org/10.1016/S0257-8972(96)02994-5
22. Cicconi MR, Giuli G, Paris E, Courtial P, Dingwell DB. XAS investigation of rare earth elements in sodium disilicate glasses, J Non-Cryst Sol. 2013;362:162–68. https://doi.org/10.1016/j.jnoncrysol.2012.11.035
23. Dingwell DB. Viscosity-temperature relationships in the system $Na_2Si_2O_5$-$Na_2Al_4O_5$. Geochim Cosmochim Acta. 1986;50:1261-65. https://doi.org/10.1016/0016-7037(86)90409-6
24. Dingwell DB, Virgo D. Viscosities of melts in the Na2O-FeO-Fe_2O_3-SiO_2 system and factors controlling relative viscosities of fully polymerized silicate melts. Geochim Cosmochim Acta. 1988;52:395–403. https://doi.org/10.1016/0016-7037(88)90095-6
25. HVG-DGG (Hüttentechnische Vereinigung der Deutschen Glasindustrie e. V.—Deutsche Glastechnische Gesellschaft e.V.). Available from: http://www.hvg-dgg.de/fileadmin/dateien/verein/Standardglas_Ia.pdf; http://www.hvg-dgg.de/fileadmin/dateien/verein/Standardglas_Ib.pdf
26. Müller D, Pereira L, Hess K-U, Dingwell DB. Influence of lanthanides on the melt viscosity and glass density of sodium disilicate. J Non-Cryst Sol. 2023;619:122565. https://doi.org/10.1016/j.jnoncrysol.2023.122565
27. Wei L, Guo L, Li M, Guo H. Calcium-magnesium-alumina-silicate (CMAS) resistant Ba_2REAlO_5 (RE = Yb, Er, Dy) ceramics for thermal barrier coatings. J Eur Ceram Soc. 2017;37:4991–5000. https://doi.org/10.1016/j.jeurceramsoc.2017.06.004
28. Cicconi MR. Europium (Eu) and Cerium (Ce) in Silicate Glasses: XAS Study of their Oxidation States and Local Environments. PhD thesis, University of Camerino. 2010. p. 226.
29. Cicconi MR, Giuli G, Paris E, Dingwell DB. Europium structural environment in a sodium disilicate glass by XAS. J Non-Cryst Sol. 2010;356:1749–53. https://doi.org/10.1016/j.jnoncrysol.2010.06.029
30. Burnham AD, Berry AJ, Halse HR, Schofield PF, Cibin G, Mosselmans JFW. The oxidation state of europium in silicate melts as a function of oxygen fugacity, composition and temperature. Chem Geol. 2015;411:248–59. https://doi.org/10.1016/j.chemgeo.2015.07.002
31. Pinet O, Phalippou J, Di Nardo C. Modeling the redox equilibrium of the Ce^{4+}/Ce^{3+} couple in silicate glass by voltammetry. J Non-Cryst Sol. 2006;362:5382–90. https://doi.org/10.1016/j.jnoncrysol.2006.08.034
32. Duffy JA. Acid-base reactions of transition metal oxides in the solid state. J Am Ceram Soc. 1997;80:1416–20. https://doi.org/10.1111/j.1151-2916.1997.tb02999.x
33. Duffy JA. Polarisability and polarizing power of rare earth ions in glass: an optical basicity assessment. Phys Chem Glass. 2005;46:1–6. https://www.ingentaconnect.com/content/sgt/pcg/2005/00000046/00000001/art00001
34. Cicconi MR, Giuli G, Paris E, Ertel-Ingrisch W, Ulmer P, Dingwell DB. Europium oxidation state and local structure in silicate glasses. Am Min. 2012;97:918–29. https://doi.org/10.2138/am.2012.4041
35. Dietzel A. Die Kationenfeldstärken und ihre Beziehungen zu Entglasungsvorgängen, zur Verbindungsbildung und zu den Schmelzpunkten von Silicaten. Zeitschrift für Elektrochemie und angewandte physikalische Chemie. 1942;48:9–23. https://doi.org/10.1002/bbpc.19420480104

36. Guo W, Wang Z, Zhao Z, An Z, Wang W. Effects of CeO_2 on the viscosity and structure of high-temperature melt of the CaO-SiO_2-(Al_2O_3)-CeO_2 system. J Non-Cryst Sol. 2020;540:120085. https://doi.org/10.1016/j.jnoncrysol.2020.120085
37. Vogel W. Glaschemie, VEB Deutscher Verlag für Grundstoffindustrie, Leipzig. 1983;434.
38. Barbieri L, Cannillo V, Leonelli C, Montorsi M, Mustarelli P, Siligardi C. Experimental and MD simulations study of CaO-ZrO_2-SiO_2 glasses. J Phys Chem B. 2003;107:6519–25. https://doi.org/10.1021/jp022551c
39. Ghosh A, Chatterjee A. Ironmaking and Steelmaking: Theory and Practice. New Delhi: PHI Learning Private Limited; 2008. p. 472.

SUPPORTING INFORMATION

Additional supporting information can be found online in the Supporting Information section at the end of this article.

How to cite this article: Müller D, Dingwell DB. Calcium–magnesium–aluminum-silicate melt viscosities influenced by lanthanides, yttrium, and zirconium. J Am Ceram Soc. 2024;1–8. https://doi.org/10.1111/jace.19646